Nature and shape of stacking faults in 3C-SiC by molecular dynamics simulations

Luca Barbisan Andrey Sarikov Anna Marzegalli Francesco Montalenti Leo Miglio*

L. Barbisan, Dr. A. Sarikov, Dr. A. Marzegalli, Prof. F. Montalenti, Prof. L. Miglio
L-NESS and Department of Materials Science, Università degli Studi di Milano-Bicocca, via R. Cozzi 55, I-20125, Milano, Italy
Email: luca.barbisan@unimib.it
Dr. A. Marzegalli
Department of Physics, Politecnico di Milano, via Anzani 42, I-22100, Como, Italy
Dr. A. Sarikov
V. Lashkarev Institute of Semiconductor Physics, National Academy of Sciences of Ukraine, 45 Nauki avenue, 03028 Kyiv, Ukraine

Keywords: *Silicon Carbide (SiC), Electronic Properties, Defect Characterization, Stacking Faults, Shockley Partial Dislocation, Dislocation Annihilation, Molecular Dynamics*

Classical molecular dynamics simulations are employed to investigate the three-dimensional evolution of stacking faults (SFs), including the partial dislocation (PD) loops enclosing them, during growth of 3C-SiC layers on Si(001). It is shown that the evolution of single PD loops releasing tensile strain during the initial carbonization stage, commonly preceding 3C-SiC deposition, leads to the formation of experimentally observed V- or Δ-shaped stacking faults, the key role being played by the differences in the mobilities between Si- and C-terminated partial dislocation segments. Nucleation in the adjacent planes of PD loops takes place at later stage of 3C-SiC deposition, when slightly compressive-strain conditions are present. It is shown that such a process very efficiently decreases the elastic energy of the 3C-SiC crystal. The maximum energy decrease is obtained via the formation of triple stacking faults with common boundaries made up by PD loops yielding a zero total Burgers vector. Obtained results explain the experimentally observed relative abundance of compact microtwin regions in 3C-SiC layers as compared to the other stacking fault related defects.

1 Introduction

Electronic industry is constantly searching for innovation technologies and new materials to be employed for realization of electronic devices. Silicon has dominated the electronic industry during the last four decades because of the possibility to implement ever increasing number of elementary devices on a single chip. This trend is known as the "Moore's law".[1] Nevertheless, the mentioned possibility is already getting close to its physical limit. Moreover, silicon has a low mobility, low saturation velocity and an indirect band-gap, which are not ideal for some applications. Therefore, a number of sectors in the electronic industry become interested in use of new semiconductor materials.
Silicon carbide (SiC) is a group IV compound that has gained interest by the electronic industry because of its high breakdown field (30×10^5 V/cm) and large saturation velocity (2×10^7 cm/s).[2] It is found in different modifications called polytypes. The most attractive for device production are two hexagonal polytypes, namely 4H-SiC and 6H-SiC, as well as the cubic one, 3C-SiC.
Cubic silicon carbide has a number of advantages over the hexagonal polytypes, such as the reduced phonon scattering as well as the highest electron mobility and saturated drift velocity.[2] Moreover, 3C-SiC layers can be heteroepitaxially grown on (100) and (111) Si substrates, enabling direct integration into the Si technology.[3] At this, however, there is a large difference between the lattice parameters of cubic silicon carbide and silicon (about 20 % at room temperature, 0.453 nm vs. 0.543 nm, respectively) as well as their thermal expansion coefficients (about 8%).[2] Hence, several types of extended defects, such as dislocations, twins and stacking faults (SFs) nucleate at or close to the 3C-SiC/Si interface and propagate into the 3C-SiC films during both the high temperature deposition and the cooling down stages, driven by the misfit strain relaxation.[4,5] Such defects hinder the possibility of obtaining high-quality crystalline 3C-SiC on Si substrates, thus reducing drastically its potential applications.
A common strategy to reduce the 3C-SiC and Si lattice misfit strain at the early stage of the Si carbide epitaxy is the so-called carbonization process, realized by a deposition of carbon-rich precursors onto

bare Si substrate under hydrogen flux.[6] As a result of this procedure, only some residual strain remains in the layer, the sign and the magnitude of this strain depend on the deposition parameters.[7] In most cases, carbonization allows to match five SiC unit cells to four Si cells at the 3C-SiC/Si interface via the formation of an ordered array of edge dislocations.[8] The carbonization step does improve the crystal quality of 3C-SiC layers, however, it does not reduce the defect density to such an extent to ensure acceptable layer quality. Specific patterning of Si substrate has been proposed in order to further decrease the amount of extended defects.[9–13] Lower SF densities are observed at the surface of 3C-SiC layers grown on undulate,[14] pyramidal-shape,[15,16] and pillar-shape patterned substrates.[9,10] At this, however, the desired defect level for device performance (10^2 cm^{-1}) has not been reached so far.[17–19]
The effectiveness of growing techniques and their optimization strictly depend on the understanding of the evolution mechanisms of SFs and terminating them partial dislocations during deposition. A number of experimentally observed phenomena related to the SF behavior have not been fully clarified in literature. In particular, self vanishing of stacking faults has been observed,[12] namely the SFs terminated by Si atoms at the surface have been found to be much more abundant and extended than those exposing C atoms (oriented in perpendicular direction to the former). While qualitative description and explanations of this phenomenon have been provided,[12] the literature is still lacking of a proper three-dimensional modeling of underlying mechanism.
We notice also that experiments clearly demonstrate an abundance of SFs grouped in two or three adjacent $\{111\}$ planes, whereas single SFs are less frequent.[20] A successive nucleation mechanism has been proposed to explain such evidence,[21] consisting in the nucleation of a partial dislocation (PD) loop at the stage of Si carbonization to release the tensile misfit strain, followed by nucleation of two additional loops in adjacent planes during the subsequent 3C-SiC deposition stage. As a result, a triple SF (also called a microtwin) is formed. The boundary of microtwin region is stabilized by a triple dislocation defect formed due to the interaction between the PDs terminating the SFs. This defect has been identified to be detrimental for the leakage current in 3C-SiC.
In this paper we exploit classical molecular dynamics (MD) to simulate the evolution of large-area SFs under the typical strain conditions encountered at different stages of 3C-SiC growth. Obtained results are used to provide an interpretation of the experimental evidences, strengthening the general understanding of defect evolution in 3C-SiC. In particular, we first clarify the mechanism resulting in different extensions and terminations of SFs at the surface. We show that the extension of a SF line at the surface is the consequence of its shape in the 3C-SiC layer bulk. One of two different shapes (Δ or V one), depending on the SF plane, is acquired by the SF during the evolution under tensile strain condition at the initial stage of Si substrate carbonization. The formation of either shape is conditioned by the difference in the motion velocities of Si- and C-terminated PD segments enclosing the SF. Then, we follow the evolution of triple SFs, analyzing their possible structures at different stages of 3C-SiC growth. In particular, we show that the nucleation of PD loop in the planes adjacent to pre-existing SFs, at the deposition stage after the carbonization, is able to very efficiently decrease the elastic energy of the 3C-SiC crystal. The maximum energy decrease is obtained via the formation of triple stacking faults with common boundaries made up by PD loops yielding a zero total Burgers vector. We finally show the atomic structures of boundary defects and the shapes of triple SFs, also known as twins.

2 Methods

The evolution of partial dislocations and stacking faults in 3C-SiC was simulated in the framework of classical molecular dynamics. Simulations were performed by exploiting the Large-scale Atomic/Molecular Massively Parallel Simulator (LAMMPS).[22] We employed the Vashishta inter-atomic potential,[23] which has some advantages over other empirical potentials fitted on SiC parameters.[24] This potential takes into account the atom interactions beyond the first neighbour shell and, because of that, provides different total energies for the hexagonal and the cubic configurations, thus enabling for an estimate of non-zero SF energies.
All simulations presented below were run in the canonical (NVT) ensemble, using a Nose-Hoover ther-

mostat.[25] The atomic trajectories were analyzed using the Open Visualization Tool (OVITO) software,[26] which allows for a very convenient analysis of the results of atomistic simulations, identifying extended defects in virtual crystals, highlighting SFs and providing dislocation lines along with the associated Burgers vectors.
Orthogonal simulation cells, oriented along the directions determined by the vectors $\boldsymbol{u} = a/2[1\bar{1}0]$, $\boldsymbol{v} = a/2[110]$, and $\boldsymbol{w} = a[100]$ were used, and periodic boundary conditions (PBC) were applied in the $\boldsymbol{u}$ and $\boldsymbol{v}$ directions. To model the effect of a thick bulk substrate below the 3C-SiC layer, the bottom three layers of the simulation cell were kept fixed to bulk positions. In order to make possible the observation of the evolution of extended dislocation loops, a large box ($38.8 \times 38.8 \times 26.0$ nm^3, corresponding to 3'369'528 atoms) was considered.
Dislocation loops were inserted in the simulation cell by shifting each atom by the displacement field vectors calculated by dislocation modelling in the framework of the linear elasticity theory.[27] The obtained configurations were geometrically optimized using a conjugated gradient minimisation algorithm. We recall that, for an arbitrary dislocation segment, the field components can be easily calculated rotating the reference system and decomposing the dislocation Burgers vector into a screw ($b_{\|}$) and an edge component ($b_{\perp}$). At this, $\hat{z}$ axis has to be oriented along the dislocation line ξ, $\hat{x}$ axis perpendicular to ξ in the glide plane, and $\hat{y}$ axis oriented following the right hand rule, respectively. In this case, the components of the displacement field vectors are written as follows:

$$u_x(x,y,z) = \frac{b_{\perp}}{2\pi}\left(\arctan(y,x) + \frac{x\,y}{2(1-\nu)(x^2+y^2)}\right) \tag{1a}$$

$$u_y(x,y,z) = -\frac{b_{\perp}}{2\pi}\left(\frac{(1-2\nu)\log(x^2+y^2)}{4(1-\nu)} + \frac{x^2-y^2}{4(1-\nu)(x^2+y^2)}\right) \tag{1b}$$

$$u_z(x,y,z) = \frac{b_{\|}}{2\pi}\arctan(y,x) \tag{1c}$$

where $\nu = 0.25$ is the Poisson ratio of 3C-SiC.[28] We did not introduce any correction of the displacement field related to the infinite image arrays of dislocation loops created by the periodic boundary conditions along the $\boldsymbol{u}$ and $\boldsymbol{v}$ directions. Each segment of our closed loop has its counterpart with opposite Burgers vector, therefore they behave like a dislocation dipole together. As a result, the stress induced by the presence of a dislocation loop decreases faster than in the case of infinite dislocation lines. However, as the stress normal to the free surface should be zero after system equilibration, the displacement field components (1a)-(1c) were corrected by adding image dislocation loop in vacuum above the free surface.[27]
For all the simulations presented in this paper the annealing of the systems was performed at the thermostat temperature of 1400 K, corresponding to the typical experimental temperature for 3C-SiC deposition. The integration time step was 1 fs, chosen as the longest possible one to ensure relative energy conservation to 10^{-5} in micro-canonical simulations. Thermal dilation of the 3C-SiC film was taken into account by scaling the simulation box dimensions. The scaling factor was calculated simulating a 3C-SiC bulk cell using the Nose-Hoover barostat.

3 Results and discussion

The evolution of SFs in silicon carbide is driven by the strain conditions which can actually change during the growth. As mentioned in the Introduction section, carbonization process is commonly used to reduce the 3C-SiC and Si misfit strain.[6] At this very first stage of 3C-SiC epitaxy a tensile strain is accumulated in the film because of 20% lattice mismatch between SiC and Si. Tensile strain is a well known source of partial dislocations. Therefore, we expect that SFs nucleate at this stage. In particular 90° Schockley partials are known to lead the tensile strain relaxation. Carbonization process induces the reconstruction of the 3C-SiC/Si interface allowing to match five SiC unit cells to four Si cells via the

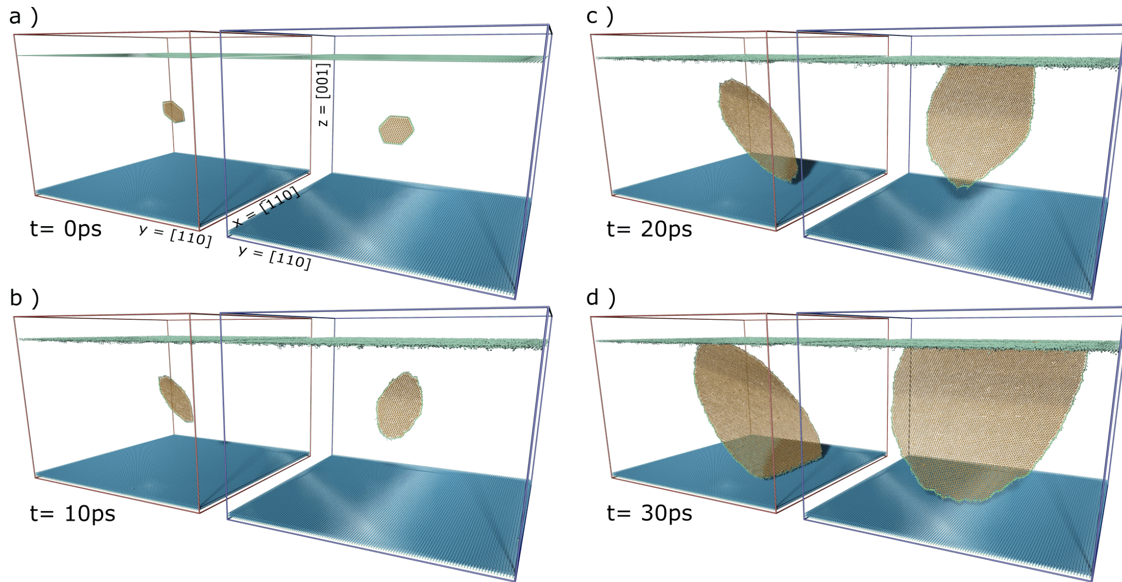

Figure 1: Classical molecular dynamics simulations snapshots of the evolution of hexagonal partial dislocation loops. Simulations were performed under bi-axial tensile strain at 1400K, computing the atomic interactions using Vashishta potential. Periodic boundary conditions are applied in x and y directions. Two simulations are analyzed in parallel. On the left (red cell) the evolution of an HPD loop that lies in a (111) plane is presented. The right panels (blue cell) show the evolution of an HPD loop lying in a ($1\bar{1}1$) plane. Only stacking faulted atoms (orange), fixed atoms (dark blue) and surface atoms (light blue) are shown for clarity. Dislocation lines, obtained with OVITO DXA algorithm are displayed as green lines bounding the SFs. Four snapshots correspond to: initial configurations (a), atomic configurations after 10 ps (b), 20 ps (c) and 30 ps (d) of simulation time.

formation of an ordered array of edge dislocations.[8] Such reconstruction leaves a slightly compressed 3C-SiC layer (at the growth temperature) for the subsequent deposition. As recently pointed out,[21] this change in the strain sign between different stages of 3C-SiC layer growth is very important for understanding the origin and the characteristics of SFs in epitaxial 3C-SiC.
We divided our results in two subsections in order to follow the strain conditions at different 3C-SiC growth stages. In the first subsection we illustrate through MD simulations how the experimentally observed shape of a single SF is resulted from the evolution of PD loop under experimental conditions.
In the second subsection we analyse the evolution of the defects presented in the first subsection when the strain changes its sign.

3.1 Evolution of SF at the initial stage of the deposition

Partial dislocations in zinc-blend crystals have preferential line directions coinciding with equivalent $<$110$>$ directions. Stacking faults lie in {111} planes, therefore PDs terminating them have six preferential equivalent $<$110$>$ directions in each plane. As a consequence, the evolution of a general-case SF can be studied starting from a closed hexagonal partial dislocation (HPD) loop formed by $<$110$>$ dislocation segments enclosing the stacking fault as shown in **Figure 1** (**a**).
Figure 1 shows the results of the MD simulations of two HPD loops evolving under an external applied bi-axial tensile strain. In the simulations, we considered a strain $\varepsilon_{xx} = \varepsilon_{yy} = 4\%$. Notice that performing simulations under the actual strain conditions experienced during growth is virtually impossible. We know that the very initial nominal strain is around 20%. However, simulations under such very high strain conditions lead to pronounced crystal disordering. Therefore, we have picked a value of strain high enough to allow us for the observation of HPD loop dynamics in a reasonable computational time.
The simulations shown in the left and the right panels of Figure 1 are identical, except for the glide plane where the HPD loop is located. On the left (red cell) the evolution of an HPD loop that lies in a (111) plane is shown, while the right panels (blue cell) show the evolution of an HPD loop lying in a ($1\bar{1}1$) plane.

We analyze the specific cases of loops releasing the tensile strain at the initial stage of the 3C-SiC growth. In terms of Burgers vector, the only choice exists for the loop to release such strain, namely when its Burgers vector forms an angle of 90° with the loop segment parallel to the 3C-SiC/Si substrate interface. In view of the crystal geometry and non-equivalence of the Si and C species in the 3C-SiC lattice, each dislocation loop comprises three segments terminated by silicon and three other segments terminated by carbon atoms. Furthermore, the Burgers vector of the loop always forms an angle 90° with one Si- and one C-terminated dislocation segment and angles of 30° with the rest of the segments (see for reference panels (**a**) and (**f**) of **Figure 2**). As shown in Figure 2 (**k**) and (**l**), the glide set of 3C-SiC presents different stacking of Si/C mono-layers depending on the considered planes (111) or $(1\bar{1}1)$. This results in the opposite terminations of PD segments of the loops located in these planes.
Under identical conditions of temperature (1400 K) and strain, the two loops expand in a very different way. The final shape of the stacking fault enclosed by the loop is determined by the relative velocities of partial dislocation segments. In 3C-SiC, the 90° PDs are faster than 30° PDs.[24,29] Therefore, the segments with the Burgers vector perpendicular to the line direction will advance, distorting the dislocation line and reshaping the loop into a diamond shape (Figure 1 panel (**b**)). At this point the loop further expands and the terminating species of PD segments play a key role in the evolution. Experimentally, silicon terminating dislocations are known to be faster than carbon ones,[30–32] so they will move through the SiC with a higher velocity, reaching the 3C-SiC/Si substrate interface or the free surface of the epitaxial layer.
The opposite half of the loop expands slowly, and the SF acquires a triangular shape. Further evolution will continue with a triangular loop-shape until the two C terminating segments finally reach the free surface or 3C-SiC film/Si substrate interface, respectively. SFs in the $(1\bar{1}1)$ and $(1\bar{1}\bar{1})$ planes have a V-shape and terminate at the free surface exposing lines of silicon atoms aligned with the [110] direction; those in the (111) and $(11\bar{1})$ planes have a Δ-shape and terminate exposing carbon atoms aligned with the $[1\bar{1}0]$ direction.
A SF terminated with C atoms shows an opposite polarity with respect to the surrounding Si-terminated surface, whereas a SF terminated with Si does not. Therefore, subsequent deposition will tend to increase the length of Si-terminated SFs and decrease the length of C-terminated SFs.[33] As a consequence the Δ and V conformation of SFs are maintained in subsequent SiC growth.
In order to further clarify the HPD evolution observed in MD simulations, Figure 2 (**a-e**) and (**f-j**) presents the sketches of the evolution of the two types of HPD loops, releasing initial tensile strain. The final shape of the stacking fault enclosed by the loop is determined by the relative velocities of the bounding partial dislocations. Panels (**a-e**) correspond to the HPD loop in the (111) and $(11\bar{1})$ glide planes, while panels (**f-j**) represent the loop in the $(1\bar{1}1)$ and $(1\bar{1}\bar{1})$ planes, respectively. These sketches are helpful to understand the progressive HPD loop evolution towards their final Δ and V-shape in the two classes of planes.

3.2 Formation of triple SFs at the deposition stage

Experimental evidences reported in literature show that SFs in 3C-SiC epitaxial layers are mostly composed by three consecutive SF planes, forming twin regions.[20] Such SFs are of particular interest because they are a potential source of leakage in 3C-SiC, whereas single-plane SFs are not.[21] In particular, the boundaries of these twinned regions are known to introduce states in the 3C-SiC band gap.[21]
In Ref.[21], a successive nucleation mechanism has been proposed, giving an insight to explain experimental evidences on the abundance of the triple SF regions. According to the proposed mechanism, initial PD loop nucleates at the carbonization stage to relax the misfit tensile strain. Two other PD loops nucleate in order to relax the compressive strain at the subsequent stage of the 3C-SiC deposition. The nucleation of the latter PD loops takes place preferentially in the planes adjacent to the former loop, which leads to the formation of a triple SF (also called a microtwin). This mechanism has been proved by MD simulations, however, taking into consideration only the evolution of infinitely-long PD loop segments parallel to the 3C-SiC/Si interface.[21] Considering an infinite dislocation line is clearly a limit for understanding the formation of triple SFs. Therefore, in this work, we make a generalization by considering

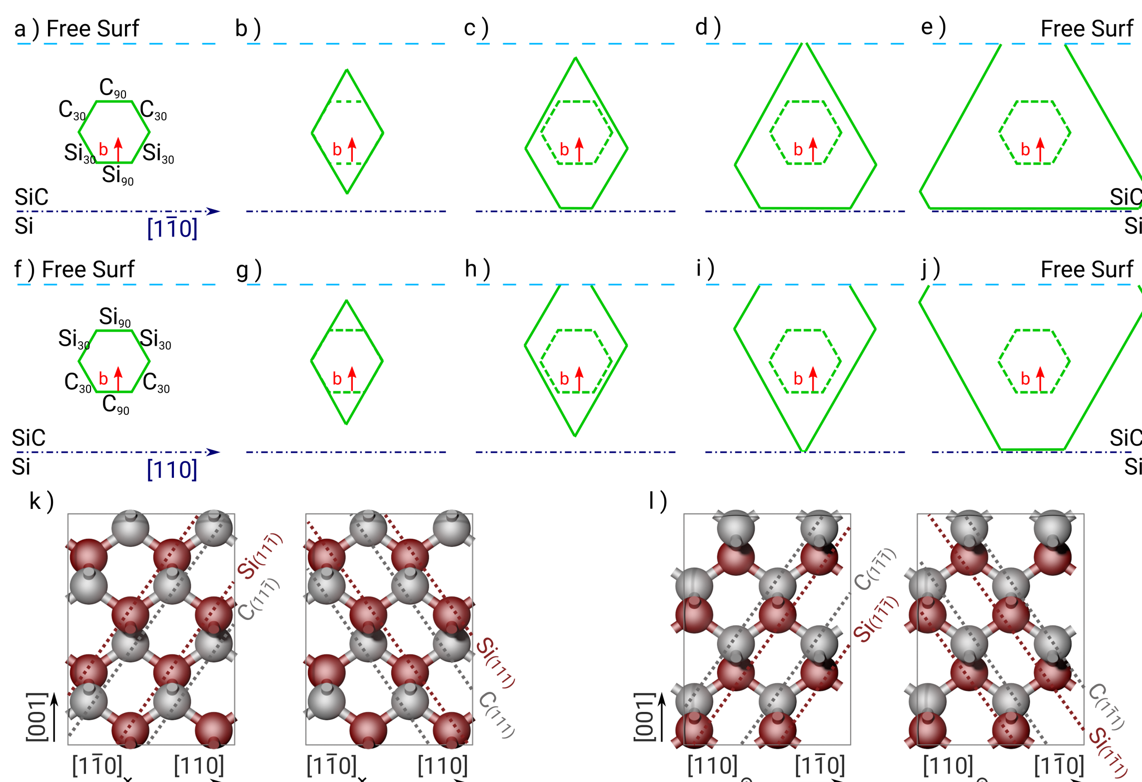

Figure 2: Diagram of the evolution of hexagonal partial dislocation loops in different glide planes. The evolution of the loops with Burgers vector <112> under tensile strain conditions is shown. Burgers vectors are displayed as red arrows. In the top row (a - e) the evolution of loops in the (11$\bar{1}$) and (111) glide planes (i.e. glide planes parallel to the [1$\bar{1}$0] direction) is shown. Middle row (f - j) shows the evolution of loops in the (1$\bar{1}$1) and (1$\bar{1}\bar{1}$) glide planes (i.e. glide planes parallel to the [110] direction). In the bottom row (k - l) the reference zinc-blend structure projected in [110] and [1$\bar{1}$0] directions is presented, relevant glide planes are highlighted by dashed lines.

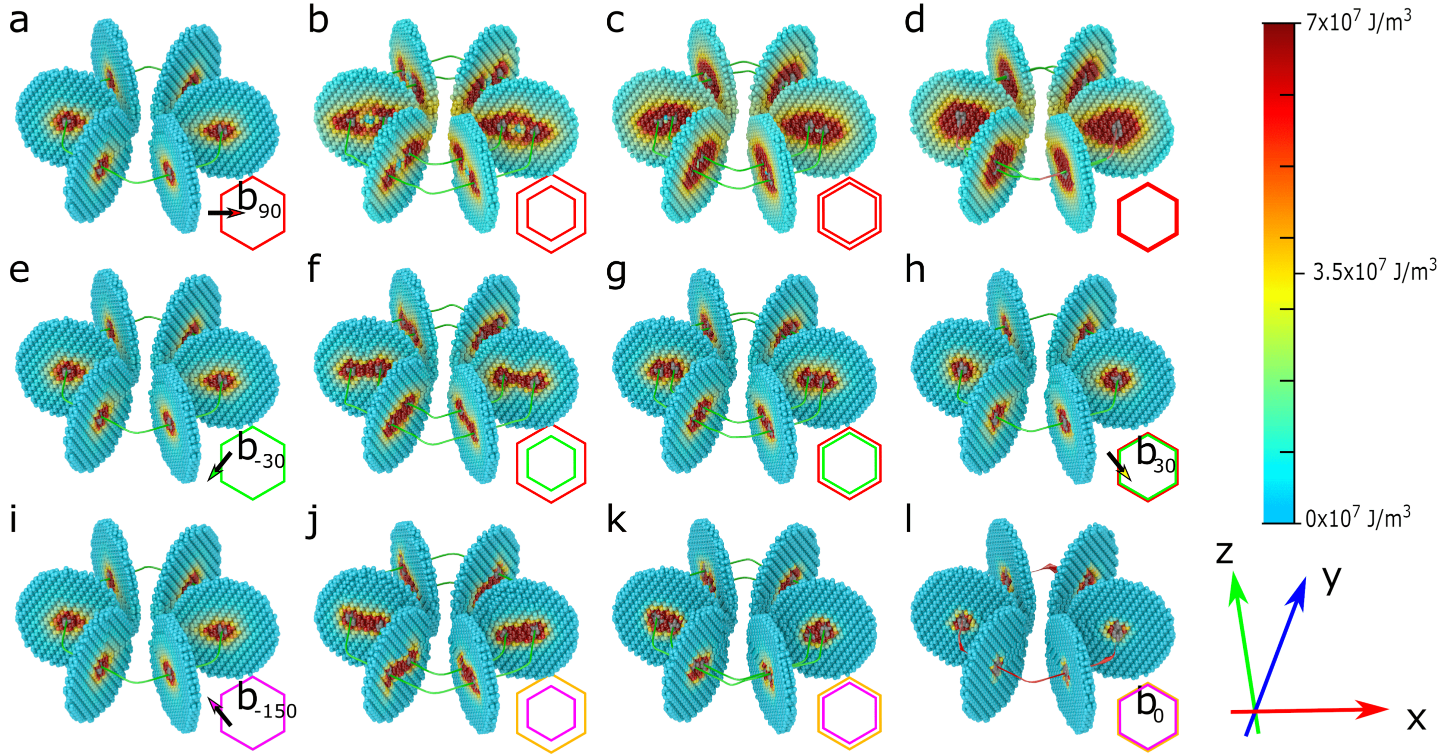

Figure 3: Elastic energy map near each segment of HPD loops. First column: maps for single HPD loop with different Burgers vectors, (**a**) elastic energy map along a loop with $\mathbf{b}_{90} = [1\bar{1}\bar{2}]$; (**e**) along a loop with $\mathbf{b}_{-30} = [121]$; (**i**) along a loop with $\mathbf{b}_{-150} = [\bar{2}\bar{1}1]$. Second to fourth column: maps for combinations of HPD loops in adjacent planes, segments of different loops are separated by a distance that varies form 1 nm (second column) to 0 nm (fourth column). For different configurations of HPD loops the difference in loop radii decreases along each row from 2nd to 4th column. (**b-d**) elastic energy map for the combination of two loops with $\mathbf{b}_{90}$; (**f-h**) combination of two loops with $\mathbf{b}_{90}$ and $\mathbf{b}_{-30}$; (**j-l**) combination of three loops with $\mathbf{b}_{90}$, $\mathbf{b}_{-30}$ and $\mathbf{b}_{-150}$, in this case loops with $\mathbf{b}_{90}$ and $\mathbf{b}_{-30}$ have the same radius because they correspond to the stable double HPD loop of panel (**h**) with $\mathbf{b}_{30} = [21\bar{1}]$.

the entire PD loops. Notice that a simulation according to the illustrated mechanism would require to reproduce nucleation. However, molecular dynamics is not able to model rare events like dislocation loop nucleation. Therefore we decided to study the possibility of a triple subsequent nucleation event in successive planes indirectly, via the analysis of the strain fields created by various HPD loop combinations. We perform a static and energetic analysis of the typical configurations of three-dimensional HPD loops, showing their structure and the associated elastic energy. This allows us to identify which PD segments tend to form common boundaries and which do not. The three-dimensional generalization of the mechanism proposed in Ref.[21] provides a clear explanation of the formation of triple SFs as a process that very efficiently relaxes the elastic energy of the system.

In panels (**a**, **e** and **i**) of **Figure 3** we show the elastic energy maps near the segments of HPD loops, each of them characterized by one of the three possible Burgers vectors. For easy reading, each HPD loop is identified by referring to its Burgers vector and the angle between the latter and the HPD loop segment parallel to the 3C-SiC/Si interface (i.e. $\mathbf{b}_{90} = [1\bar{1}\bar{2}]$, $\mathbf{b}_{-30} = [121]$, $\mathbf{b}_{-150} = [\bar{2}\bar{1}1]$). The reference directions are $y = [110]$, $x = [\bar{1}12]$ and $z = [1\bar{1}1]$. They correspond to (y) an arbitrary dislocation line direction in the (001) plane, (x) the perpendicular direction inside the glide plane and (z) the direction normal to loop plane, respectively.

The initial tensile strain can be reduced by the HPD loop shown in Figure 3 (**a**), while a compressive strain can be released by the two loops in Figure 3 (**e**, **i**). Let's consider first the hypothesis of a double SF originated from two HPD loop with the same Burgers vector $\mathbf{b}_{90}$ (i.e. both nucleated under tensile strain conditions as proposed in Ref.[34]). Panels (**b-d**) of Figure 3 show how the elastic energy increases as the segments of the two loops become close each to other. In effect their strain fields overlap so that the compressed/dilated regions near each segment become superimposed, dramatically increasing

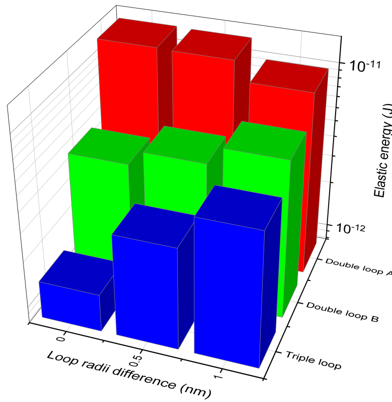

Figure 4: Elastic energy of three combinations of HPD loops as a function of the difference between the loop radii: red bars represent the elastic energy of two HPD loops in adjacent planes, both loops having $\mathbf{b}_{90}$; green bars show the elastic energy of two HPD loops in adjacent planes, one with $\mathbf{b}_{90}$, the other with $\mathbf{b}_{-30}$; blue bars correspond to the elastic energy of three HPD loops in adjacent planes, one with $\mathbf{b}_{90}$, one with $\mathbf{b}_{-30}$ (with the same radius), one with $\mathbf{b}_{-150}$.

the elastic energy (panel (**d**)). As a consequence, the formation of a multiple SF by identical PD loops in adjacent planes turns out to be unfavorable. Moreover, no common boundary of such multiple SF is possible as the bounding PDs would not overlap, because for them it's energetically favorable to remain separated.

The situation is different when the second loop has different Burgers vector, such as $\mathbf{b}_{-30}$ or $\mathbf{b}_{-150}$, and relaxes a compressive strain. As demonstrated in Ref.[21], once the strain is changed after the carbonization step, the nucleation of loops with the mentioned Burgers vectors is enhanced, especially in the planes adjacent to the first SF. In this case the interaction between the SF boundaries is attractive,[35] as shown in Figure 3 (**f-h**) for loops with $\mathbf{b}_{90}$ and $\mathbf{b}_{-30}$. The elastic energy decreases as the segments of the two loops approach each other. The most favorable configuration is when all the segments join together, forming a double SF and an HPD loop with Burgers vector $\mathbf{b}_{30} = [21\bar{1}]$, the sum of the ones of the two HPD loops. For these segments it is energetically favorable to lock into a single defect. This explains why a unique boundary is observed around multiple SFs instead of separated PD segments.[35,36] The difference in this latter case from the case of two loops with the same Burgers vectors considered above is that compressed regions near each segment overlap with the dilated regions of the other loop and vice-versa. The enhancement is stronger if the two loops are situated in adjacent planes, because the compression/dilation is stronger in the equatorial plane of the loop.

The HPD loop surrounding the double SF shown in panel (**h**) of Figure 3 has a Burgers vector which is exactly the opposite to the other suitable choice for Burgers vector for single HPD loop to release compressive strain ($\mathbf{b}_{30}$ and $\mathbf{b}_{-150}$, respectively). A triple SF can be formed if the latter HPD loop nucleates in a plane adjacent to the double SF, therefore it is of particular interest to analyze such loop interaction. Panels (**j-l**) of Figure 3 show how the elastic energy decreases as the segments of the two loops become closer. The elastic energy is dramatically reduced when all the segments meet. Therefore, formation of the triple SF with a sharp boundary according to the discussed mechanism is energetically favorable.

The elastic energy for configurations shown in panels (**b-d**, **f-h**, **j-l**) of Figure 3 is shown in **Figure 4**. The elastic energy is plotted as a function of the difference between the loop radii. In Figure 4, the difference of the loop radii decreases in each row from 2nd to 4th column. In the case of two HPD loops with the same Burgers vector (red bars, "double loop A" in Figure 4), the elastic energy increases when the loop segments approach. The elastic energy decreases only in the case of HPD loops with different Burgers vectors (green bars, "double loop B" in Figure 4) and is dramatically reduced in the case of three loops with three different Burgers vectors (blue bars, "triple loop" in Figure 4).

Obtained results enable us to summarize the mechanism of the formation of triple stacking faults during growth of 3C-SiC layers as follows. First, an HPD loop releasing the tensile strain nucleates during

stage of carbonization. Once the strain has changed to compressive one at the 3C-SiC deposition stage, an HPD loop releasing such strain nucleates in one of the adjacent planes of already existing SF. Finally, a third HPD loop also releasing compressive strain and having Burgers vector opposite to the one of the existing double SF, nucleate in the other adjacent plane, eventually forming a micro-twin. In view of our results, the most favorable evolution of later generated SFs is to expand so to form a unique, common dislocation boundary with already existing SFs. The boundary of single HPD loops nucleated under tensile strain conditions will acquire the Δ- or V-shape, as demonstrated in the Section 3.1. It is reasonable to suppose therefore that the boundary of the multiple SFs will acquire the same shapes. The nucleation of HPD loops under compressive strain condition at the stage of 3C-SiC deposition makes the difference, transforming single SFs into multiple SFs and stabilizing them.
In **Figure 5** we illustrate three-dimensional views of the Δ- and V-shape structure of triple stacking faults formed in two classes of glide planes considered here. These structures have been obtained inserting three trapezoidal PD loops in three adjacent glide planes followed by geometrical optimization of structure with a conjugated gradient algorithm using the Vashishta potential. The central PD in each structure has a Burgers vector corresponding to relaxation of tensile strain. The dislocation boundaries of the other two SFs that sandwich the middle one have two different Burgers vectors corresponding to the compressive strain relaxation. The boundary dislocation defects of these two triple SFs are displayed in the circular insets of the Figure 5. Atomic configurations of these defects are of particular interest because some of them may introduce states in the 3C-SiC band gap,[21] being therefore the source of the leakage currents in epitaxially grown 3C-SiC layers.

4 Conclusions

In this paper we have analyzed the formation of the shapes of single stacking faults in epitaxial 3C-SiC layers on Si substrates. Via molecular dynamics simulations, we have shown for the first time the three-dimensional evolution of PD loops enclosing the SFs.
The stress field present in the layer due to the lattice mismatch with the substrate, drives the increase of the loop radius in order to increase the size of relaxed region in the system. Loop segments close to the interface are forced to reach it and to deposit a misfit segment while the segments near the surface are attracted to it and expelled, allowing the loop to transform in a semi-loop. The exact shape acquired by the loop is determined by relative segment velocities. Silicon-terminated PDs are faster than carbon-terminated ones and 90° PDs are faster than 30° ones. Because of the difference in terminating species of the loop segments between the upper- and lower-half of the loop, the loop acquires a V- or Δ-shape, when the faster Si-terminated segments reach the 3C-SiC free surface or the 3C-SiC/Si interface, respectively. As a result, V-shaped SFs appear whenever the the core element of the dislocation segment near the interface is C and Δ-shaped SFs appear when that terminating specie is silicon. The correspondence with the experimental results is evident,[12] and the simulations highlight how crucial is the concurrence in the expansion velocities.
Moreover, taking into account our previous studies, we propose the mechanism to explain the abundance of triple SF in 3C-SiC layers observed experimentally. It has been demonstrated in our previous publication,[21] that successive nucleation mechanism can explain the experimental evidence of an abundance of multiple SF in 3C-SiC, in particular for thick films.[20] However, this mechanism was described only for infinite, straight dislocation lines. In this work, we have extended this mechanism to a more general case of hexagonal partial dislocation loops. Elastic energy maps were provided, illustrating the strong interaction between the PD segments delimiting SFs. Our analysis confirms that the most probable mechanism for the formation of multiple SFs is that they originate only in the vicinity of pre-existing SFs, which have nucleated to release misfit tensile strain. The most convenient path for generating multiple SFs is to nucleate PD loops able to relax a compressive strain, which is possible only in a different stage of the 3C-SiC growth with respect to the stage when the nucleation of single SFs happened. A direct implication is that multiple SFs would acquire the shape of the pre-existing SF in this case. Our interpretation is fully supported by experimental evidences.[12] Finally, we propose the minimum energy config-

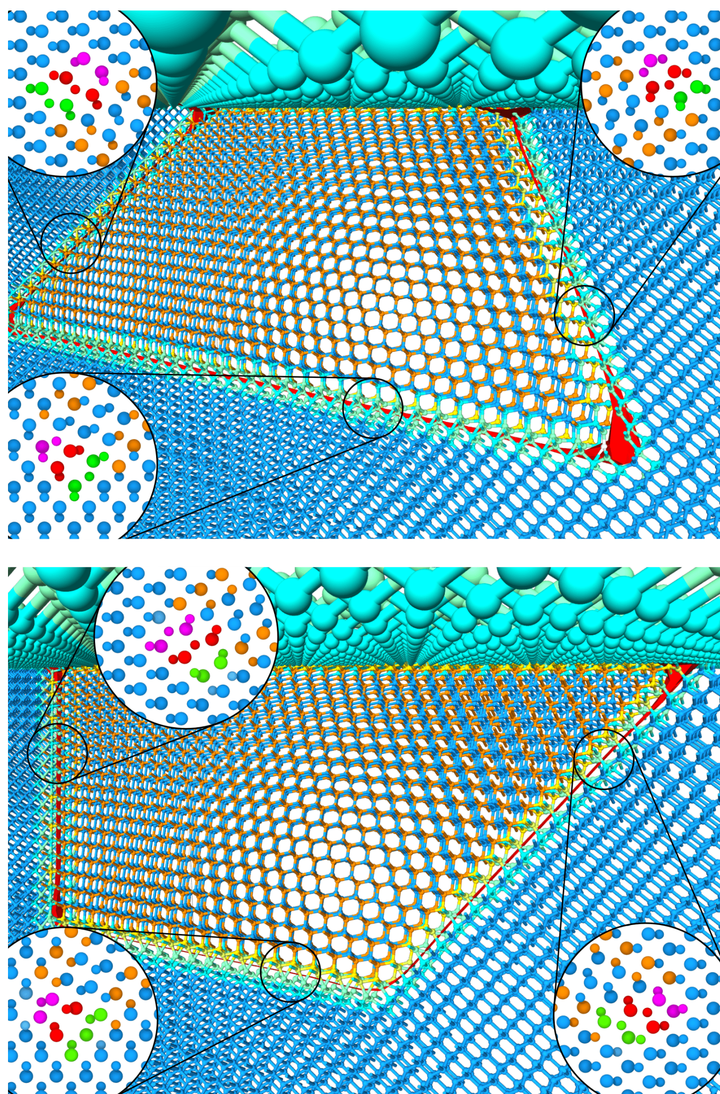

Figure 5: Shape and terminations of triple SFs. Top: SF shape in the (111) and $(11\bar{1})$ planes; Bottom: SF shape in the $(1\bar{1}1)$ and $(1\bar{1}\bar{1})$ planes. The dislocation line is colored in red. In the circles the core structures projected on the planes perpendicular to the line direction are highlighted. Core atoms are colored to indicate the Burgers vector of the dislocation in the respective plane: each color correspond to a different Burgers vector, with the same nomenclature of Figure 3. Blue sticks and atoms correspond to zinc-blend structure, orange ones to wurzite structure. Lighter hues are used in the defect surroundings

urations for the triple SFs (twin) in the V- and Δ- shape, providing the core structure of their boundary segments.
The first set of results about the single-dislocation loop can help in the optimization of the deposition of 3C-SiC layers on patterned Si substrates allowing to set up a strategy to enhance SF annihilation. The second set of results may be used for following-on analysis of the impact of dislocation complexes on the electronic properties of the 3C-SiC layers. As demonstrated in Ref.[21], the knowledge of the specific core structures is required for superior ab initio calculations of their electronic properties, therefore, our results provide the input for such calculations.

Acknowledgements
The authors acknowledge EU for funding the CHALLENGE project (3C-SiC Hetero-epitaxiALLy grown on silicon compliancE substrates and 3C-SiC substrates for sustaiNable wide-band-Gap power devices) within the EU's H2020 framework program for research and innovation under grant agreement no. 720827.

Conflicts of interest
There are no conflicts to declare.

References

[1] G. E. Moore, *IEEE Solid-State Circuits Society Newsletter* **2006**, *11*, 3 33.

[2] G. Harris, *Properties of Silicon Carbide*, EMIS datareviews series. INSPEC, Institution of Electrical Engineers, **1995**.

[3] S. Nishino, J. A. Powell, H. A. Will, *Appl. Phys. Lett.* **1983**, *42*, 5 460.

[4] P. Pirouz, C. M. Chorey, T. T. Cheng, J. A. Powell, *MRS Proceedings* **1987**, *91* 399.

[5] M. E. Levinshtein, S. L. Rumyantsev, M. S. Shur, *Properties of advanced semiconductor materials: GaN, AIN, InN, BN, SiC, SiGe*, Wiley, **2001**.

[6] S. Nishino, *J. Electrochem. Soc.* **1980**, *127*, 12 2674.

[7] G. Ferro, T. Chassagne, A. Leycuras, F. Cauwet, Y. Monteil, *Chem. Vap. Deposition* **2006**, *12*, 8-9 483.

[8] C. Wen, Y. M. Wang, W. Wan, F. H. Li, J. W. Liang, J. Zou, *J. Appl. Phys.* **2009**, *106*, 7 073522.

[9] H. von Känel, L. Miglio, D. Crippa, T. Kreiliger, M. Mauceri, M. Puglisi, F. Mancarella, R. Anzalone, N. Piluso, F. La Via, *Mater. Sci. Forum* **2015**, *821-823* 193.

[10] M. Meduňa, T. Kreiliger, I. Prieto, M. Mauceri, M. Puglisi, F. Mancarella, F. La Via, D. Crippa, L. Miglio, H. von Känel, *Mater. Sci. Forum* **2016**, *858* 147.

[11] R. Anzalone, C. Bongiorno, A. Severino, G. D'Arrigo, G. Abbondanza, G. Foti, F. La Via, *Appl. Phys. Lett.* **2008**, *92*, 22 224102.

[12] H. Nagasawa, M. Abe, K. Yagi, T. Kawahara, N. Hatta, *Phys. Status Solidi B* **2008**, *245*, 7 1272.

[13] R. Vasiliauskas, M. Marinova, M. Syväjärvi, E. Polychroniadis, R. Yakimova, *J. Cryst. Growth* **2014**, *395* 109 .

[14] Y. Sun, S. Izumi, S. Sakai, K. Yagi, H. Nagasawa, *Mater. Sci. Forum* **2012**, *717-720* 501.

[15] G. D'Arrigo, A. Severino, G. Milazzo, C. Bongiorno, N. Piluso, G. Abbondanza, M. Mauceri, G. Condorelli, F. La Via, *Mater. Sci. Forum* **2010**, *645* 135.

[16] M. Zimbone, M. Zielinski, C. Bongiorno, C. Calabretta, R. Anzalone, S. Scalese, G. Fisicaro, A. La Magna, F. Mancarella, F. La Via, *Materials* **2019**, *12*, 20.

[17] C. Wen, Y. M. Wang, W. Wan, F. H. Li, J. W. Liang, J. Zou, *J. Appl. Phys.* **2009**, *106*, 7 073522.

[18] M. Bosi, C. Ferrari, D. Nilsson, P. J. Ward, *CrystEngComm* **2016**, *18* 7478.

[19] M. A. Capano, A. Smith, B. C. Kim, E. Kvam, S. Tsoi, A. Ramdas, J. A. Cooper, *Mater. Sci. Forum* **2006**, *527* 431.

[20] H. Nagasawa, R. Gurunathan, M. Suemitsu, *Mater. Sci. Forum* **2015**, *821* 108.

[21] E. Scalise, L. Barbisan, A. Sarikov, F. Montalenti, L. Miglio, A. Marzegalli, *J. of Mater. Chem. C* **2020**, *8* 8380.

[22] S. Plimpton, *J. Comput. Phys.* **1995**, *117*, 1 1 .

[23] P. Vashishta, R. K. Kalia, A. Nakano, J. P. Rino, *J. Appl. Phys.* **2007**, *101*, 10 103515.

[24] A. Sarikov, A. Marzegalli, L. Barbisan, E. Scalise, F. Montalenti, L. Miglio, *Model. Simul. Mater. Sc.* **2019**, *28*, 1 015002.

[25] W. Shinoda, M. Shiga, M. Mikami, *Phys. Rev. B* **2004**, *69* 134103.

[26] A. Stukowski, *Model. Simul. Mater. Sc.* **2009**, *18*, 1 015012.

[27] J. Hirth, J. Lothe, *Theory of Dislocations*, Krieger Publishing Company, **1982**.

[28] L. Tong, M. Mehregany, L. G. Matus, *Appl. Phys. Lett.* **1992**, *60*, 24 2992.

[29] A. T. Blumenau, C. J. Fall, R. Jones, S. Öberg, T. Frauenheim, P. R. Briddon, *Phys. Rev. B* **2003**, *68* 174108.

[30] B. Chen, J. Chen, T. Sekiguchi, T. Ohyanagi, H. Matsuhata, A. Kinoshita, H. Okumura, F. Fabbri, *Superlattices Microst.* **2009**, *45*, 4-5 295.

[31] S. Ha, M. Skowronski, H. Lendenmann, *J. Appl. Phys.* **2004**, *96*, 1 393.

[32] S. I. Maximenko, T. S. Sudarshan, *J. Appl. Phys.* **2005**, *97*, 7 074501.

[33] H. Nagasawa, K. Yagi, T. Kawahara, N. Hatta, M. Abe, *Microelectron. Eng.* **2006**, *83*, 1 185 .

[34] Y. Sun, S. Izumi, S. Sakai, K. Yagi, H. Nagasawa, *Comp. Mater. Sci.* **2013**, *79* 216 .

[35] A. Sarikov, A. Marzegalli, L. Barbisan, F. Montalenti, L. Miglio, *Materials* **2019**, *12*, 18 3027.

[36] M. Zimbone, A. Sarikov, C. Bongiorno, A. Marzegalli, V. Scuderi, C. Calabretta, L. Miglio, F. La Via, *Acta Mater.* **2020**, submitted.

Table of Contents

a) Evolution of single plane stacking faults in 3C-SiC

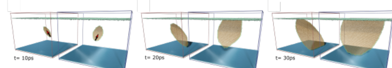

b) Elastic energy of partial dislocation loop for multiple stacking faults

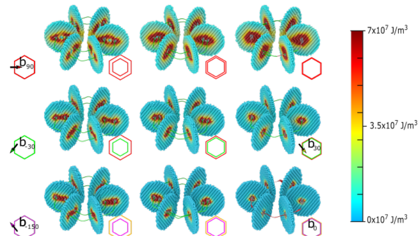

The paper deals with molecular dynamics simulations of the three-dimensional evolution of stacking faults enclosed by partial dislocation loops, at different stages of the epitaxial growth of 3C-SiC layers on Si substrates. The mechanisms of stacking fault shaping as well as preferential formation of twin regions made up by three stacking faults lying in consecutive lattice planes, are revealed.